
SBP-YOLO: A LIGHTWEIGHT REAL-TIME MODEL FOR DETECTING SPEED BUMPS AND POTHOLES

Chuanqi Liang¹ Jie Fu¹ Lei Luo¹ Miao Yu^{1*}

¹Key Laboratory for Optoelectronic Technology and Systems, Ministry of Education,
College of Optoelectronic Engineering, Chongqing University, Chongqing, China
20230801037@stu.cqu.edu.cn, fujie@cqu.edu.cn, llei@cqu.edu.cn, yumiao@cqu.edu.cn

August 5, 2025

Abstract

With the increasing demand for ride comfort from occupants of new energy vehicles, accurate and real-time detection of speed bumps and potholes has become critical for predictive suspension control. This paper presents SBP-YOLO, a lightweight detection framework built upon YOLOv11, optimized for embedded deployment. The proposed model integrates GhostConv for efficient computation, VoVGSCSPC for enhanced multi-scale feature representation, and a Lightweight and efficiency detection head (LEDH) to reduce the cost of early-stage feature processing. A hybrid training strategy combining NWD loss, knowledge distillation, and Albumentations-based weather augmentation is employed to improve detection accuracy and robustness, particularly for small and distant targets. Experimental results demonstrate that SBP-YOLO attains an 87.0% mAP, surpassing the baseline YOLOv11n by 5.8%, while achieving 139.5 FPS on the Jetson AGX Xavier platform following TensorRT FP16 quantization. This performance reflects substantial improvements in inference speed and computational efficiency. The findings validate the proposed method's effectiveness for real-time road condition perception in intelligent suspension systems.

1 Introduction

With the rapid emergence of new energy vehicles (NEVs) as a mainstream transportation mode, consumers are placing increasingly higher demands on ride comfort and handling stability [1]. Compared to traditional internal combustion engine vehicles, electric vehicles (EVs) feature faster response times and smoother torque output, which pose greater challenges for the dynamic performance of suspension systems [2]. To ensure smooth driving and a comfortable experience under complex road conditions, real-time road condition perception has become critically important. Road surface irregularities such as speed bumps and potholes are primary factors affecting vehicle dynamics and ride comfort [3], as these disturbances are transmitted through the suspension system to the vehicle body, directly impacting passenger experience. The key to advanced suspension control lies in the anticipatory perception and accurate prediction of road disturbances, including the classification of stochastic road profiles and the identification of impulse-type irregularities [4]. Intelligent suspension systems, leveraging previewed road information, can dynamically adjust stiffness and damping to adapt to complex road environments. This enables effective suppression of vehicle body vibrations and attitude changes, thereby enhancing driving stability and safety [5, 6]. In EVs in particular, the rapid torque response of electric motors imposes greater demands on the perception and reaction speed of suspension systems. This is particularly critical when encountering sudden road irregularities such as potholes and speed bumps, which require swift and precise adaptation. Consequently, more tightly coordinated integration with the overall vehicle dynamics is essential to maintain both ride comfort and driving safety.

Real-time detection of road surface anomalies remains a technical challenge. Traditional methods rely on vehicle dynamics, image processing, or costly sensor setups [7, 8]. Dynamics-based approaches analyze acceleration and vibration signals under varying road conditions to identify anomalies such as speed bumps and potholes. For instance, Celaya-Padilla et al. [9] introduced a sensor-fusion-based method for speed bump detection, employing gyroscope,

*Corresponding author: yumiao@cqu.edu.cn

accelerometer, and GPS data, with a logistic model optimized via cross-validation and genetic algorithms. Salman et al. [10] used smartphone sensors with CNN-LSTM models to detect and classify speed bumps with up to 98.92% accuracy. Similarly, Yin et al. [11] proposed a smartphone-based approach utilizing acceleration and GPS data, where signal preprocessing and an Extracted Data Feature Filter (EDFF) were applied to effectively differentiate between potholes and speed bumps. Aguilar-González et al. [12] developed a random forest classifier using tri-axial vibration data for road event detection. Despite their effectiveness, these methods are typically task-specific and computationally expensive, lacking the predictive capability required for real-time suspension control in intelligent vehicles.

In recent years, the rapid development of deep learning has significantly advanced object detection techniques based on computer vision, providing new solutions for identifying road surface anomalies such as speed bumps and potholes. Compared with conventional methods relying on accelerometer signals, deep learning-based vision approaches enable proactive perception of road surface conditions, allowing earlier and more accurate detection of anomalies for suspension predictive control. The YOLO (You Only Look Once) series is widely utilized in road surface anomaly detection [13], offering a favorable trade-off between detection accuracy and inference speed, which is critical for real-time perception in intelligent vehicles. For example, Park et al. [14] conducted a comparative study of three YOLO variants, namely YOLOv4, YOLOv4-tiny, and YOLOv5s, and concluded that YOLOv4-tiny provided the most favorable trade-off between real-time performance and detection accuracy for pothole recognition. ASAD et al. [15] implemented a lightweight Tiny-YOLOv4 model on a Raspberry Pi device for edge-based pothole detection, achieving a detection accuracy of 90% at 31.76 FPS. Khan et al. [16] introduced a YOLOv8-based real-time pothole detection method for autonomous vehicles, outperforming YOLOv5 on public datasets through data augmentation. To address challenges caused by variable lighting and adverse weather conditions, Bučko et al. [17] constructed a dataset containing road images captured under different environmental scenarios and validated the performance of the YOLOv3 algorithm accordingly. Furthermore, Bhavana et al. [18] proposed POT-YOLO based on YOLOv8, capable of detecting various pavement anomalies such as cracks, oil stains, patches, and cobblestones, achieving a detection accuracy of 97.6%. These studies highlight the effectiveness of YOLO-based detection algorithms in real-time identification of road anomalies under complex driving conditions.

Despite progress in vision-based detection of potholes and speed bumps, real-world use under dynamic driving remains difficult. At long range, these anomalies appear small, making them hard to detect. Motion blur from fast driving degrades features, while shadows, glare, and dim lighting obscure road cues and reduce robustness. Limited computing power on embedded systems also limits input size and model depth, making real-time use harder. To address these challenges, this paper proposes a lightweight and efficient model tailored for speed bump and pothole detection. The main contributions are as follows:

- LEDH is proposed to alleviate the overhead of the P2 detection layer, maintaining accuracy for small, distant targets while reducing head complexity from dense, high-dimensional convolutions.
- GhostConv modules are applied to the backbone and neck for efficient feature extraction, while VoVGSCSPC improves robustness across varying road and environmental conditions.
- To improve detection of small and distant targets in dynamic environments, a comprehensive training strategy is adopted, integrating NWD Loss [19] for accurate localization, BCKD [20] for knowledge distillation, and Albumentations-based [21] augmentation to simulate motion blur, lighting changes, and adverse weather, enhancing robustness and generalization.
- Quantized to FP16 and optimized with TensorRT, the model achieves 139.5 FPS inference speed on the NVIDIA Jetson AGX Xavier, meeting strict latency demands for real-time road detection and enabling reliable embedded deployment.

2 Methods

2.1 SBP-YOLO

YOLOv11 [22] is the latest advancement in the YOLO series of object detection frameworks, integrating the C3k2 block, SPP-Fast module, and the parallel spatial attention C2PSA block, which collectively enhance feature extraction and detection performance. The series includes multiple variants ranging from lightweight to large-scale models; this study selects the lightweight YOLOv11n as the baseline to meet the real-time and computational constraints of embedded platforms. However, existing models still face challenges in handling multi-scale targets and complex backgrounds, especially in accurately detecting small and distant road anomalies such as potholes and speed bumps. To mitigate these limitations, this paper proposes the SBP-YOLO model Fig. 1: GhostConv modules replace standard convolutions (SC) in the deeper network layers to reduce computational cost while preserving strong feature extraction; the VoVGSCSPC module enhances multi-scale feature representation; a dedicated P2 detection layer and LEDH are designed to improve

small-object detection; The overall network architecture is annotated with output feature map dimensions, such as (320, 320, 16), representing height, width, and channel depth, to clearly illustrate the scale of features at each stage.

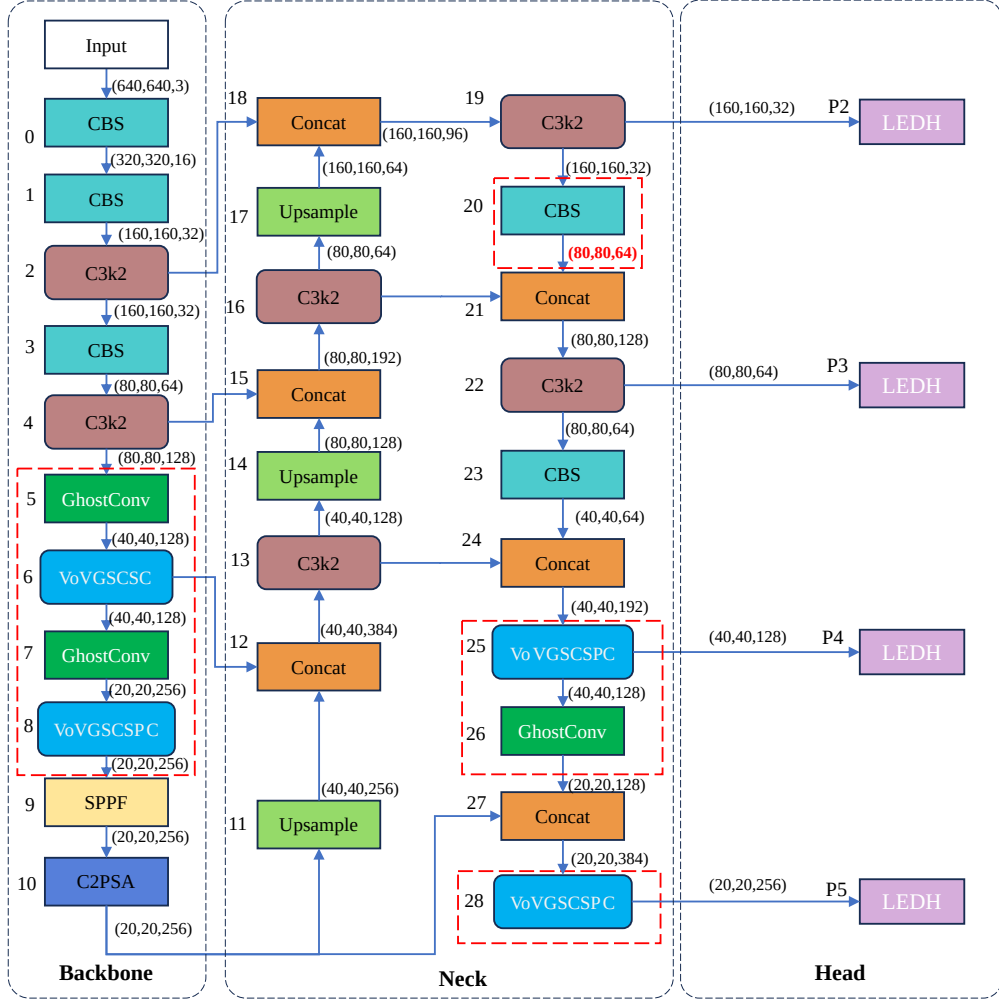


Figure 1: SBP-YOLO framework with Backbone, Neck, and Head. The Neck fuses multi-scale features (P2–P5) from the Backbone and passes them to the Head for classification and regression

2.2 GhostConv

Standard convolutional (SC) modules often generate redundant feature maps, resulting in high computational and memory costs. To mitigate this, the GhostConv module from GhostNet [23] generates additional “ghost” feature maps through inexpensive operations, effectively reducing complexity while preserving representational capacity. As illustrated in Fig. 2, GhostConv employs a two-step process: first, intrinsic feature maps are produced by SC with small kernels; subsequently, 5×5 depthwise convolutions (DWConv) expand these to approximate the full feature set. The outputs from both steps are fused, delivering comparable results to SC but with substantially fewer parameters and reduced computation. By applying DWConv to only half of the channels, GhostConv efficiently enlarges the receptive field and lowers computational overhead.

Let c_1 and c_2 be the input and output channels, k the kernel size, and $H \times W$ the input feature map dimensions. Ignoring bias, the parameter count P_{Conv} and FLOPs F_{Conv} of a SC are:

$$P_{\text{Conv}} = c_1 c_2 k^2, \quad F_{\text{Conv}} = 2c_1 c_2 H W k^2. \quad (1)$$

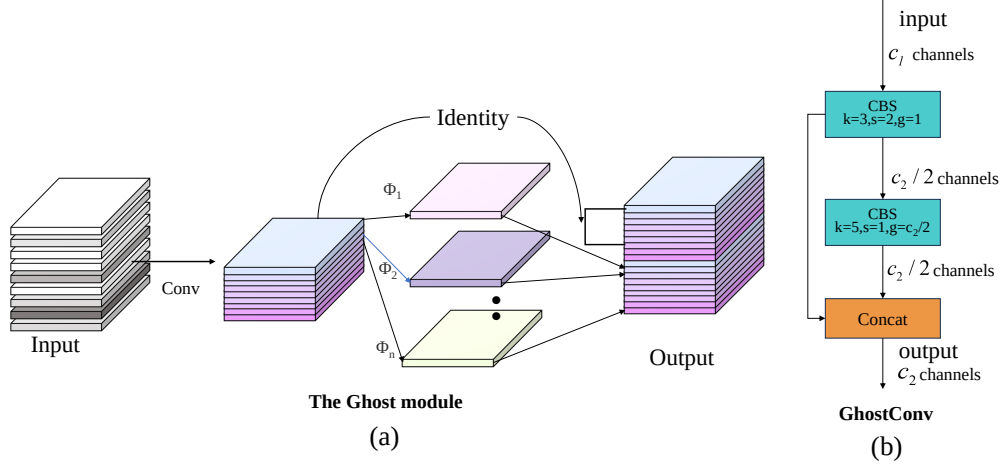


Figure 2: GhostConv structure diagram

In GhostConv, the main convolution produces half of the output channels, $\frac{c_2}{2}$, followed by a cheap convolution generating the remainder. The total parameter count P_g and computational cost F_g are:

$$P_g = c_1 \frac{c_2}{2} k_m^2 + \frac{c_2}{2} k_c^2, \quad F_g = c_1 c_2 H W k_m^2 + c_2 H W k_c^2, \quad (2)$$

where k_m and k_c denote the kernel sizes of the main and cheap convolutions, respectively. For example, at SBP-YOLO's 7th layer, the GhostConv module reduces theoretical computation to 51.1% and parameter count by 48.9% compared to SC, markedly decreasing model complexity and size.

2.3 VoVGSCSPC

Depthwise separable convolution (DSConv) reduces computational cost and parameters by decomposing SC into depthwise convolution (DWConv) for spatial filtering and pointwise convolution (PWConv) for channel mixing. However, since spatial and channel information are processed separately in DWConv, inter-channel information exchange is limited, leading to feature isolation within groups. To mitigate this issue, ShuffleNets [24] introduced the channel shuffle operation to enable cross-channel interaction, while MobileNet [25] employed extensive 1×1 dense convolutions to fuse channel information. Nevertheless, the dense 1×1 convolutions increase the computational burden. Although channel shuffle and other lightweight operations improve efficiency, their performance remains inferior to SC.

GSConv [26] addresses these limitations by integrating the advantages of GhostConv with a hardware-friendly, efficient channel shuffle mechanism. This design overcomes the information isolation problem inherent in DWConv, enabling efficient intra-group feature flow and enhancing feature representation and overall model performance. GSConv not only reduces computational complexity but also improves cross-group feature fusion, achieving accuracy comparable to or exceeding SC in lightweight networks. This makes GSConv a promising solution for high-performance visual tasks on mobile and embedded platforms. As shown in Fig. 3, GSConv first applies a SC for downsampling, followed by a DWConv on the resulting features. The outputs are concatenated and shuffled to produce the final feature map:

$$F_{\text{GSC}} = \text{Shuffle}(\text{Cat}(\alpha(X_{C_1})_{C_2/2}, \delta(\alpha(X_{C_1})_{C_2/2})))_{C_2} \quad (3)$$

where X_{C_1} is the input with C_1 channels, α denotes SC, δ represents DWConv, and F_{GSC} indicate the output.

VoVGSCSPC extends GSConv with a cross-stage design, splitting the input into two branches: one with a convolution followed by a GSBN, and another with a DWConv residual branch. Their outputs are fused as

$$GSB_{\text{out}} = F_{\text{GSC}}(F_{\text{GSC}}(\alpha(X_{C_1})_{C_1/2})) + \alpha(X_{C_1})_{C_1/2} \quad (4)$$

$$VoVGSCSP_{\text{out}} = \alpha(\text{Concat}(GSB_{\text{out}}, \alpha(X_{C_1}))) \quad (5)$$

where GSB_{out} and $VoVGSCSP_{\text{out}}$ denote intermediate and final outputs, respectively.

The VoVGSCSPC module, employed instead of the C3k2 modules in the backbone and neck, enhances multi-scale feature fusion and enriches semantic representation. This improvement enables the model to better capture both global and local context in images of potholes and speed bumps, thereby strengthening its perceptual and representational capabilities.

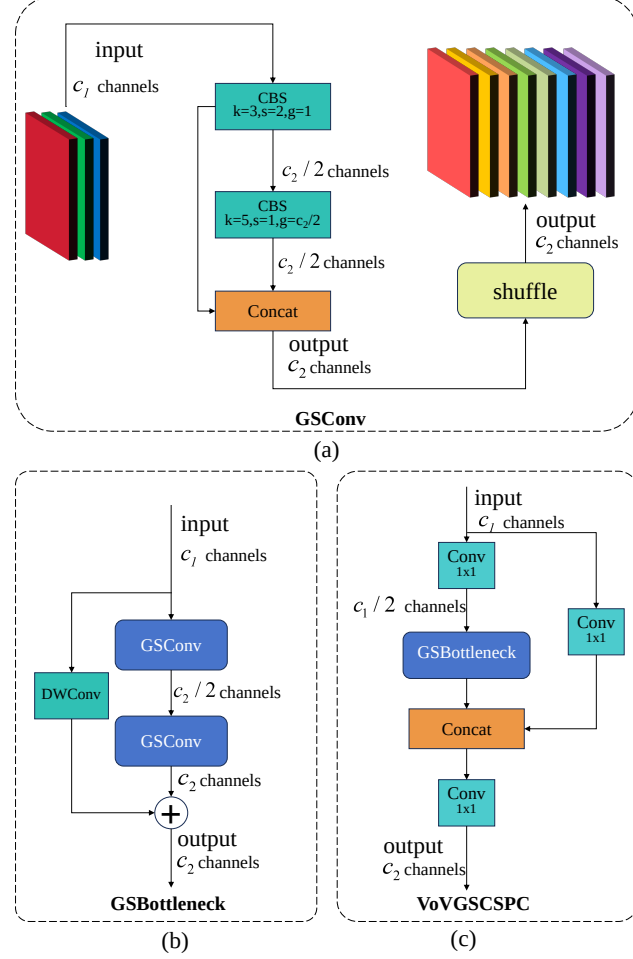
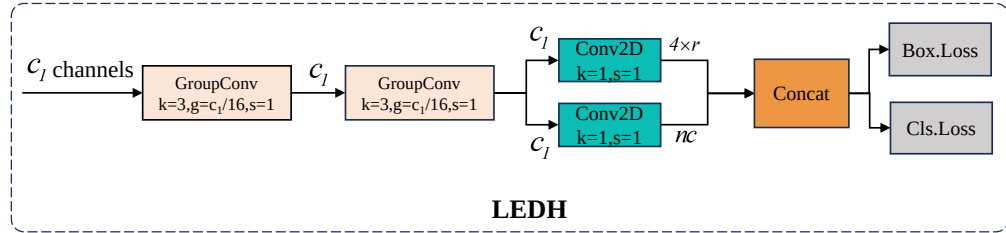


Figure 3: The flowchart of the VoVGSCSPC

2.4 Lightweight and efficiency detection head (LEDH)

In suspension preview control, road anomalies such as speed bumps and potholes often appear as small, low-saliency objects at a distance, posing typical small object detection challenges. Although the inclusion of a shallow P2 detection layer in YOLOv11 enhances detection performance for such targets, it also introduces considerable computational overhead, hindering deployment on resource-constrained edge devices. In response to this challenge, we propose the LEDH, which preserves accuracy on small targets while significantly reducing computational complexity, enabling real-time inference in embedded systems. As shown in Fig. 4, LEDH adopts a decoupled architecture with parallel

Figure 4: Lightweight and efficiency detection head (LEDH) structure. Inputs P2, P3, P4, and P5 go through 3×3 GroupConv and two Conv2D layers, then concat into two branches for classification and regression to yield predictions

branches for classification and regression. To enhance feature expressiveness with minimal cost, each branch includes

two stacked 3×3 grouped convolutions with group count $g = c_i/16$, applied to the input feature \mathbf{x}_i at scale i :

$$\begin{aligned} F_i &= \text{Conv}_g(\text{Conv}_g(\mathbf{x}_i)), \\ H_i &= \text{Concat} [\text{Conv}_{1 \times 1}^{4r}(F_i), \text{Conv}_{1 \times 1}^{n_c}(F_i)] \end{aligned} \quad (6)$$

where F_i denotes the enhanced feature, while H_i represents the final prediction output, consisting of box regression logits and class probabilities. The terms n_c and r refer to the number of classes and the DFL bin count, respectively. LEDH processes multi-scale features (P2–P5) from the backbone, enriching both spatial resolution and semantic depth through grouped convolutions. This structure reduces parameter count and FLOPs while preserving receptive field and non-linear capacity. Final predictions are produced via lightweight 1×1 convolutions for classification and bounding box regression. The design balances detection accuracy and computational efficiency, particularly benefiting small-object detection tasks under edge deployment constraints.

2.5 Hybrid Loss Training Strategy

In road scene images, small structures such as speed bumps and potholes often appear with low pixel occupancy and blurred boundaries. This makes IoU-based losses highly sensitive to minor localization errors and insufficient for robust supervision. To mitigate this problem, we introduce the normalized Wasserstein distance (NWD) [19] as a distribution-aware metric, which models both predicted and ground truth boxes as 2D Gaussian distributions. NWD provides smoother gradients under positional shifts and better tolerance to scale variation. By combining NWD with conventional IoU loss, the model gains improved localization precision, especially for small objects. Given bounding boxes $A = (cx_a, cy_a, w_a, h_a)$ and $B = (cx_b, cy_b, w_b, h_b)$, the squared 2-Wasserstein distance between their corresponding Gaussian distributions \mathcal{N}_a and \mathcal{N}_b is computed. Since this distance does not directly serve as a similarity measure, it is normalized as:

$$\text{NWD}(\mathcal{N}_a, \mathcal{N}_b) = \exp \left(-\frac{\sqrt{W_2^2(\mathcal{N}_a, \mathcal{N}_b)}}{C} \right), \quad (7)$$

where C is a dataset-specific scaling constant (e.g., 0.5) determined via ablation studies. The final bounding box regression loss is defined as:

$$\begin{cases} L_{\text{NWD}} = 1 - \text{NWD}(\mathcal{N}_a, \mathcal{N}_b) \\ L_{\text{obj}} = (1 - \alpha) \cdot L_{\text{NWD}} + \alpha \cdot L_{\text{iou}} \end{cases} \quad (8)$$

where L_{NWD} represents the Wasserstein-based loss, L_{iou} is the standard IoU loss, and $\alpha = \text{IoU}_{\text{ratio}} \in [0, 1]$ controls the loss weighting.

3 Experiments and Analysis

3.1 Experimental settings

The experiments were conducted on Ubuntu 24.04 with an Intel® Xeon E5-2680 CPU (2.4 GHz) and an NVIDIA Tesla V100 GPU (16 GB). The software environment comprised PyTorch 1.13.1 and CUDA 11.7. The model was trained using the Adam optimizer with an initial learning rate of 0.001, batch size of 16, and 300 epochs. Input images were resized to 640×640 to enhance convergence and computational efficiency. Early stopping was employed, terminating training if validation performance did not improve for 30 consecutive epochs.

3.2 Dataset construction

Existing road surface datasets provide usable samples of potholes and speed bumps, but often lack comprehensive coverage of diverse driving conditions, such as varying lighting, occlusion, and road textures. To address this, we construct a targeted dataset by aggregating and refining relevant samples from multiple public sources, including benchmark datasets [17, 27–29] and community platforms such as Kaggle and Roboflow Universe. The resulting dataset captures representative road anomalies across complex real-world scenes, offering a more diverse and challenging benchmark for training and evaluating road perception models. Representative examples are shown in Fig. 6.

To further enhance generalization, data augmentation is applied to simulate challenging weather conditions such as rain and snow using efficient image transformation techniques [21]. Additional augmentations include random flipping and photometric adjustments (e.g., brightness, contrast, saturation), as illustrated in Fig. 5. The final dataset consists of 7,500 images, divided into 5,250 for training, 1,125 for validation, and 1,125 for testing.

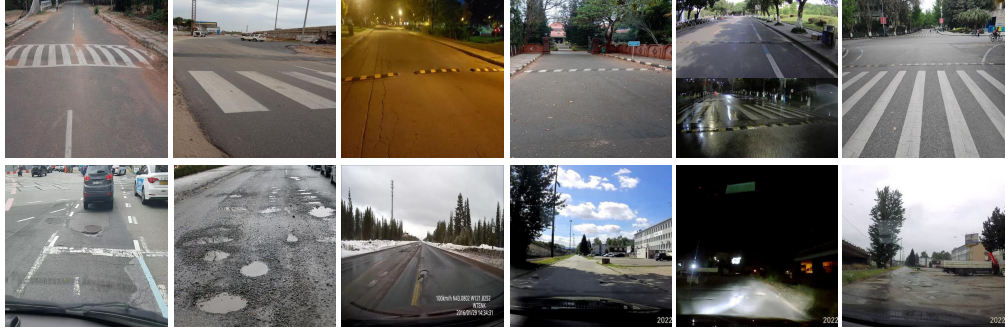


Figure 5: Images of potholes and speed bumps in the dataset



Figure 6: Comparison of the effects after some image data augmentation

3.3 Evaluation indicators

To quantitatively assess detection performance, we adopt mean average precision (mAP), including mAP at 50% IoU (mAP₅₀) and the average over IoU thresholds from 50% to 95% (mAP₅₀₋₉₅). Model efficiency is evaluated using the number of parameters (Params), GFLOPs, frames per second (FPS), and inference latency. Higher mAP reflects better detection accuracy, while higher FPS and lower latency indicate stronger real-time capability. GFLOPs and Params quantify computational and memory costs, which are critical for deployment on edge devices.

The evaluation metrics are defined as:

$$P = \frac{TP}{TP + FP}, \quad R = \frac{TP}{TP + FN} \quad (9)$$

$$AP = \int_0^1 P(R) dR, \quad mAP = \frac{1}{M} \sum_{i=1}^M AP_i \quad (10)$$

where TP , FP , and FN denote true positives, false positives, and false negatives, respectively. P and R represent precision and recall, and M is the number of object categories.

3.4 Ablation experiment

Ablation studies in Table 1 evaluate the effectiveness of each proposed module by incrementally integrating them into the YOLOv11n baseline. Each configuration includes all modules from the previous row plus one newly added component.

The baseline YOLOv11n model demonstrates fast inference (71.2 FPS) but relatively limited detection accuracy (mAP₅₀ = 81.2%, mAP₅₀₋₉₅ = 47.7%), primarily due to the absence of low-level feature information critical for detecting small objects. Introducing a P2 detection head notably improves accuracy to mAP₅₀ = 83.9%, although this

Table 1: Ablation study by sequentially adding each module on top of the baseline. Each configuration includes all modules from the previous row plus the newly added component.

Model	P (%)	R (%)	mAP ₅₀	mAP ₅₀₋₉₅	GFLOPs	Params (M)	FPS
Baseline (YOLOv11n)	85.0	75.0	81.2	47.7	6.3	2.58	71.2
+ P2 Head	84.8	76.5	83.9	49.8	10.3	2.67	53.5
+ LEDH (replacing P2)	86.6	77.6	84.5	50.1	6.7	2.37	69.6
+ GhostConv	86.3	78.1	84.5	49.8	6.2	2.09	66.5
+ VoVGSCSPC	87.5	79.2	84.6	49.9	5.8	2.04	63.7
+ NWD Loss (Final)	89.0	79.4	86.6	51.1	5.8	2.04	63.7

comes at the cost of increased computational complexity (FLOPs rise from 6.3G to 10.3G) and a drop in inference speed to 53.5 FPS.

To achieve a better accuracy-efficiency trade-off, we replace the standard P2 head with the proposed LEDH. This substitution yields further improvements in precision (+1.8%) and recall (+1.1%), while significantly reducing FLOPs by 35% and improving speed to 69.6 FPS.

Subsequently, the incorporation of GhostConv reduces the FLOPs by an additional 7.5% with minimal impact on detection accuracy. Building on this, the integration of the VoVGSCSPC backbone module not only reduces model complexity (to 5.8 GFLOPs and 2.04M Params), but also improves detection accuracy to mAP₅₀ = 84.6%.

Finally, the application of the NWD Loss further enhances the model’s ability to localize small and irregular objects, achieving the highest precision (89.0%) and overall detection performance (mAP₅₀ = 86.6%, mAP₅₀₋₉₅ = 51.1%) among all configurations. These results validate that each proposed component contributes to performance gains, and the final model presents a compelling balance of speed, accuracy, and lightweight design, making it well-suited for real-time road anomaly detection in resource-constrained environments.

3.5 Knowledge Distillation Experiment

Knowledge Distillation (KD) transfers knowledge from a larger, well-trained teacher model to a lightweight student model, aiming to enhance generalization with minimal computational overhead. The proposed KD framework adopts a hybrid strategy, integrating logit-level supervision using BCKD [20] and feature-level guidance via CWD [30]. Six corresponding intermediate layers are selected from both models to enable effective feature alignment. The detailed training hyperparameters are summarized in Table 2.

Table 2: Hyperparameter settings for the proposed Knowledge Distillation (KD) framework

Hyperparameter	Value
Training Epochs	500
Batch Size	32
Optimizer	SGD
Logits Distillation Loss	BCKD
Feature Distillation Loss	CWD
Distillation Loss Schedule	Constant
Logits Loss Weight	0.5
Feature Loss Weight	0.5
Teacher Layers Used	12, 15, 18, 21, 24, 27
Student Layers Matched	12, 15, 18, 21, 24, 27

In our study, a teacher model with similar architecture and S-level scale (20.6 GFLOPs, 7.42M Params) was employed to guide the training of the student model. As shown in Table 3, knowledge distillation leads to consistent improvements across all metrics. In particular, mAP₅₀₋₉₅ increased by 3.5% on the validation set and 3.4% on the test set, indicating not only enhanced detection performance but also improved generalization. The comparable gains across both sets suggest that the student model benefits from the teacher’s guidance without exhibiting overfitting.

Table 3: Performance comparison of distilled model, teacher model, and non-distilled baseline on validation and test sets

Validation Set	P (%)	R (%)	mAP ₅₀	mAP ₅₀₋₉₅
Baseline (Student)	89.0	79.4	86.6	51.1
+ Distillation	90.2	80.7	87.0	54.6
Teacher Model	91.0	81.4	87.4	53.8
Test Set	P (%)	R (%)	mAP ₅₀	mAP ₅₀₋₉₅
Baseline (Student)	88.6	78.2	86.3	51.5
+ Distillation	89.9	81.8	87.7	54.9
Teacher Model	89.9	82.0	87.8	54.1

3.6 Model comparison experiment

To comprehensively evaluate detection quality and computational efficiency, we compare SBP-YOLO with representative YOLO variants (YOLOv5–YOLOv12) across standard performance and complexity metrics. As reported in Table 4, SBP-YOLO achieves an mAP₅₀ of 86.6%, surpassing the YOLOv11n baseline by 5.4%, while reducing model parameters, FLOPs, and storage by 20.9%, 7.9%, and 17.9%, respectively. With knowledge distillation, SBP-YOLO (Distilled) further improves detection accuracy, reaching 87.0% mAP₅₀ and 54.6% mAP₅₀₋₉₅, without introducing additional computational overhead. These results highlight the effectiveness of our architecture and training strategy in achieving a strong trade-off between accuracy and efficiency.

To further illustrate model performance during training, Fig. 7 presents the mAP₅₀ and bounding box loss curves over 300 epochs. SBP-YOLO demonstrates consistently higher detection accuracy and lower training loss compared to other YOLO variants, indicating superior convergence speed and training stability. These trends further validate the effectiveness and robustness of SBP-YOLO for real-world deployment.

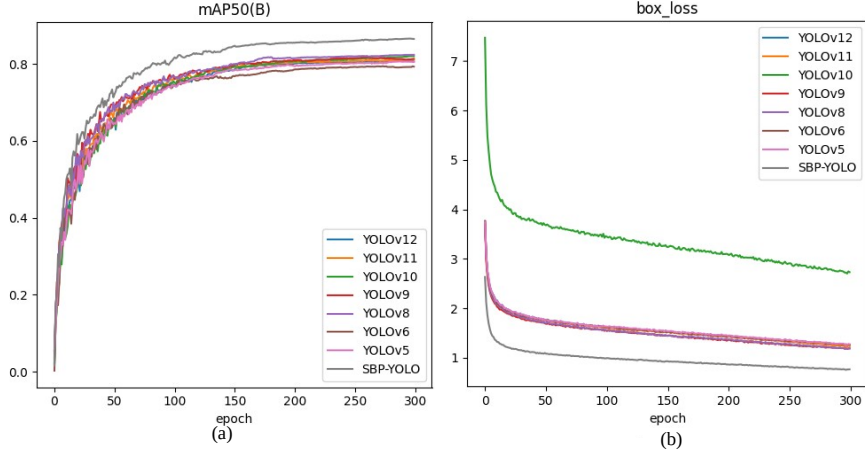


Figure 7: Training curves over 300 epochs for different YOLO models: (a) mAP₅₀, (b) bounding box loss.

3.7 Performance Comparison

As shown in Fig. 8a, SBP-YOLO exhibits improved detection capability for small-scale road features at extended distances, such as far-field speed bumps and potholes. These targets often appear with reduced resolution and weak texture cues, posing challenges to existing detection models. Compared to baseline YOLO variants, SBP-YOLO achieves higher accuracy and greater consistency in identifying such long-range and low-visibility objects. Fig. 8b illustrates detection performance under varied illumination conditions, including sunset, nighttime, and intense sunlight. SBP-YOLO maintains stable accuracy across all scenarios. At night, it outperforms YOLOv5 by 9%, and during sunset—where reduced contrast can hinder detection—SBP-YOLO shows more robust results than other models. Under strong sunlight that induces glare, SBP-YOLO successfully identifies distant potholes, whereas models like YOLOv8 occasionally miss the target. To assess robustness under visually degraded environments, Fig. 8c reports results on augmented datasets simulating rain, snow, and motion blur. SBP-YOLO achieves 0.64 detection accuracy in

Table 4: Comparison of SBP-YOLO with state-of-the-art YOLO models in terms of accuracy and efficiency

Models	P (%)	R (%)	mAP ₅₀	mAP ₅₀₋₉₅	Params (M)	GFLOPs	Size (MB)
YOLOv5n [31]	83.4	74.5	80.6	46.1	2.18	5.8	4.43
YOLOv6n [32]	83.8	72.0	79.3	45.9	4.16	11.5	8.15
YOLOv8n [33]	88.2	73.5	82.4	48.3	2.68	6.8	5.36
YOLOv9t [34]	84.7	75.3	81.5	48.3	1.76	6.6	3.95
YOLOv10n [35]	84.8	72.5	82.0	48.3	2.27	6.5	5.48
YOLOv11n [22]	85.0	75.0	81.2	47.7	2.58	6.3	5.21
YOLOv12n [36]	84.1	74.2	80.9	47.5	2.56	6.3	5.25
SBP-YOLO (ours)	89.0	79.4	86.6	51.1	2.04	5.8	4.28
SBP-YOLO (distilled)	90.2	80.7	87.0	54.6	2.04	5.8	4.28

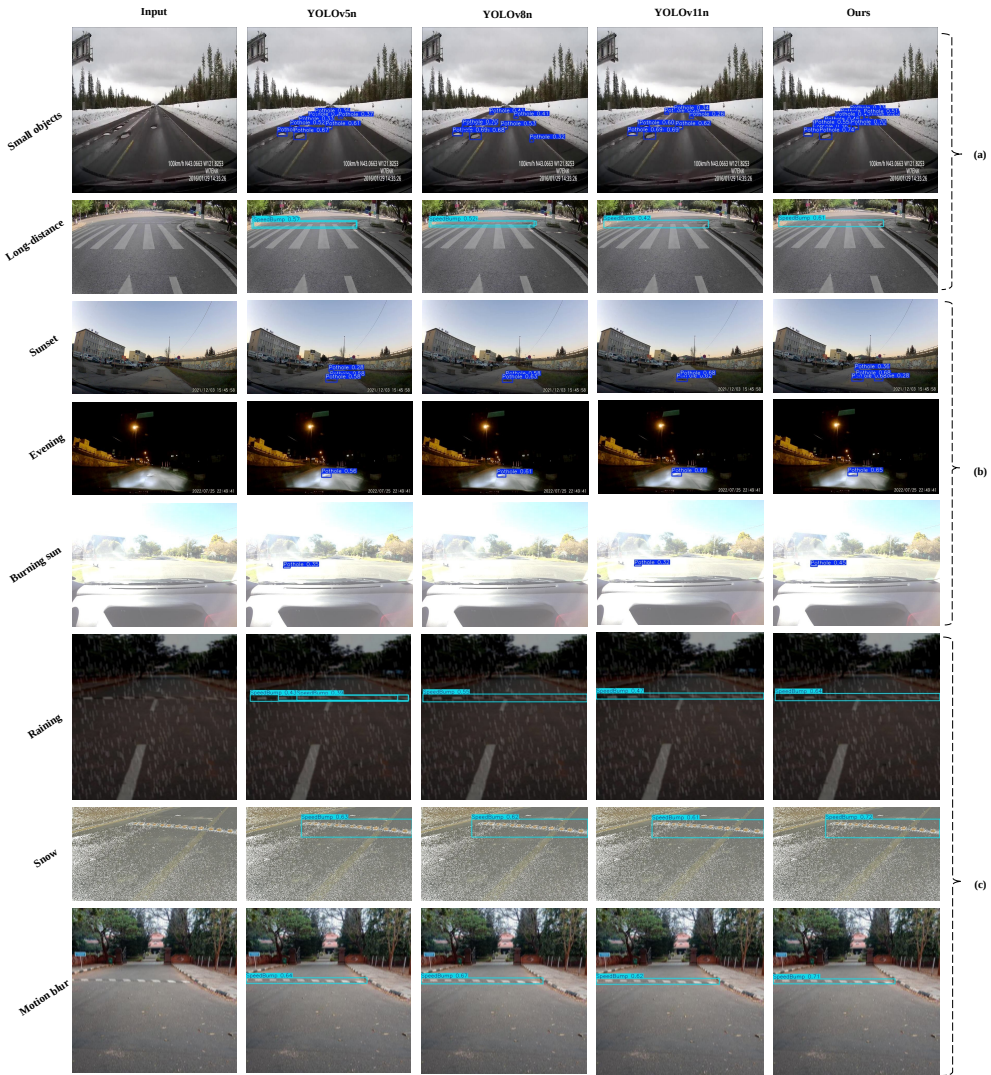


Figure 8: Qualitative comparison of SBP-YOLO and baseline models under challenging conditions: (a) detection of small distant road features; (b) robustness across varied lighting (sunset, night, strong sunlight); (c) performance under simulated rain, snow, and motion blur.

simulated rain, outperforming YOLOv11n (0.47) and YOLOv5n (lowest). Similar improvements are observed under snow and motion blur conditions, demonstrating the model's resilience across complex visual perturbations. These results demonstrate that SBP-YOLO provides a reliable and efficient solution for real-time detection of road surface features such as potholes and speed bumps. By identifying these geometric irregularities in advance, the model supports early adjustment of suspension parameters through feedforward control, helping to improve ride comfort and vehicle stability. This capability is particularly beneficial on complex or uneven roads, where timely perception is essential for safe and adaptive suspension behavior.

4 Experiment in embedded device

4.1 Experimental Environment

All embedded inference experiments were conducted on the NVIDIA Jetson AGX Xavier platform. As illustrated in Fig. 9, the experimental setup comprises the AGX Xavier module along with its carrier board. Inference was executed via the command line, enabling real-time monitoring of processing speed through the system terminal. The proposed SBP-YOLO model was converted and deployed using TensorRT, with the aid of an open-source optimization tool for YOLO models [37]. The software stack was based on NVIDIA JetPack 5.1.5.

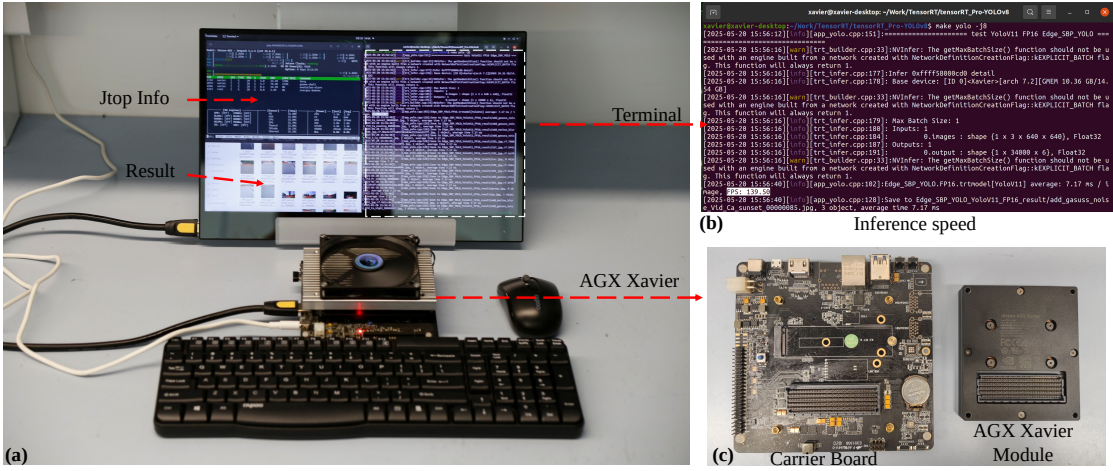


Figure 9: Experimental Hardware Platform

4.2 Inference Experiments

To ensure a fair comparison, the baseline YOLOv11n model was augmented with a P2 detection head to align with the detection structure of SBP-YOLO. As a result, the performance evaluation focuses solely on the effectiveness of the proposed improvements in SBP-YOLO, rather than differences in model capacity or detection granularity. Table 5 and Fig. 10 report the inference performance across various precision modes, including INT8, FP16, and FP32. Under FP16, SBP-YOLO achieves a 15.39 FPS gain over the modified YOLOv11n; with FP32, the improvement is 13.52 FPS. Additionally, SBP-YOLO maintains a smaller model size across all configurations, reflecting its superior efficiency. When comparing different quantization modes under identical inference conditions, INT8 yields lower accuracy and frequent missed detections. FP16 maintains accuracy close to FP32, while significantly reducing latency. Notably, SBP-YOLO under FP16 consistently detects both long-range speed bumps and complex potholes, demonstrating a lower missed detection rate and higher reliability in real-time deployment scenarios.

5 Conclusion

This paper presents SBP-YOLO, a lightweight and efficient object detection framework designed for real-time detection of speed bumps and potholes to facilitate predictive control in intelligent suspension systems. Building upon the YOLOv11 architecture, SBP-YOLO introduces a P2 detection head to improve sensitivity to small and distant targets, integrates GhostConv and VoVGSCSPC modules for efficient multi-scale feature extraction, and adopts proposed LEDH to reduce computational overhead without compromising accuracy. To further enhance robustness and generalization

Table 5: Inference time, frame rate, and model size comparison between SBP-YOLO and YOLOv11n (with P2 head) under different quantization settings.

Models	Infer Time (ms)	FPS	Weights
YOLOv11n (INT8)	6.514	152.9	5.53 MB
YOLOv11n (FP16)	8.06	124.11	7.42 MB
YOLOv11n (FP32)	14.18	70.54	14.35 MB
SBP-YOLO (INT8)	6.42	155.78	5.24 MB
SBP-YOLO (FP16)	7.17	139.50	6.18 MB
SBP-YOLO (FP32)	11.9	84.06	9.63 MB

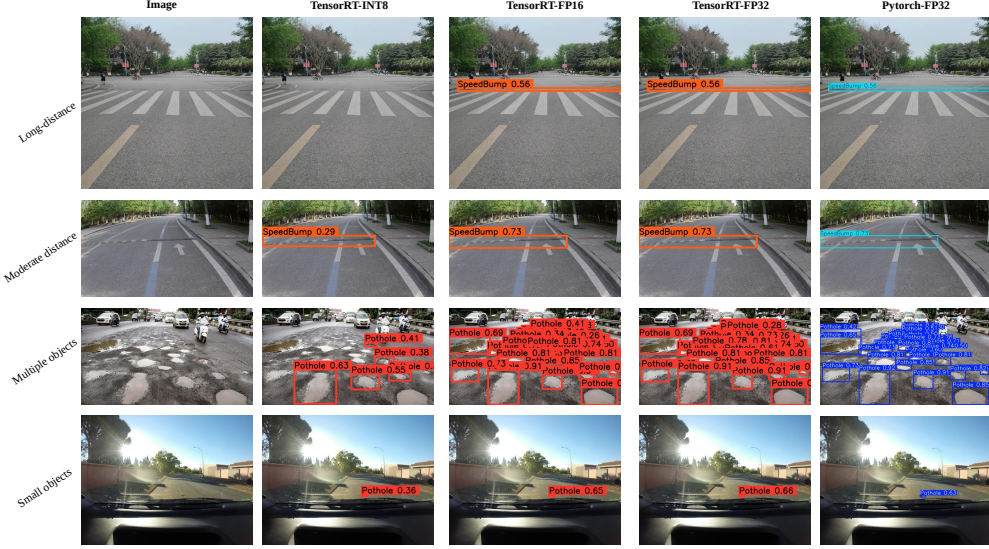


Figure 10: Comparison of recognition performance of different TensorRT quantization methods

in dynamic environments, a hybrid training strategy is employed, combining NWD loss, backbone-level knowledge distillation (BCKD), and Albumentations-based augmentation. This strategy yields consistent improvements in detection performance, particularly for small-scale anomalies, outperforming the YOLOv11n baseline by 5.8% in mAP. Experimental results show that, following TensorRT FP16 optimization, SBP-YOLO achieves 139.5 FPS on the Jetson AGX Xavier platform, representing a 12.4% increase in inference speed compared to the baseline YOLOv11n model with the same P2 detection head structure (124.1 FPS). This confirms the efficiency advantage of the presented architectural enhancements for embedded real-time deployment in intelligent suspension systems.

References

- [1] Fanchao Liao, Eric Molin, and Bert Van Wee. Consumer preferences for electric vehicles: a literature review. *Transport Reviews*, 37(3):252–275, 2017.
- [2] Zichen Zheng, Shu Wang, Xuan Zhao, Qiang Yu, Haichuan Zhang, Yang Lv, and Jia Tian. Adaptive model predictive control of four-wheel drive intelligent electric vehicles based on stability probability under extreme braking conditions. *IEEE Transactions on Intelligent Vehicles*, 2024.
- [3] Sicen Guo, Yu Jiang, Jiahang Li, Dacheng Zhou, Shuai Su, Mohammad Junaid Bocus, Xingyi Zhu, Qijun Chen, and Rui Fan. Road environment perception for safe and comfortable driving. *Autonomous driving perception: Fundamentals and applications*, pages 357–387, 2023.
- [4] Asma Achnib and Olivier Sename. Discrete-time multi-model preview control: Application to a real semi-active automotive suspension system. *Control Engineering Practice*, 137:105553, 2023.
- [5] Wei Li, Huijun Liang, Dongbin Xia, Jie Fu, and Miao Yu. Explicit model predictive control of magnetorheological suspension for all-terrain vehicles with road preview. *Smart Materials and Structures*, 33(3):035037, 2024.

[6] Guohong Wang, Farong Kou, Pengtao Liu, Wenhua Lv, and Longlong Xing. Road preview method for active suspension based on reinforcement learning. *Measurement Science and Technology*, 36(3):036206, 2025.

[7] Thiago Rateke, Karla A Justen, Vito F Chiarella, Antonio C Sobieranski, Eros Comunello, and Aldo Von Wangenheim. Passive vision region-based road detection: A literature review. *ACM Computing Surveys (CSUR)*, 52(2):1–34, 2019.

[8] Vidas Žuraulis, Vytenis Surblys, and Eldar Šabanovič. Technological measures of forefront road identification for vehicle comfort and safety improvement. 2019.

[9] Jose M Celaya-Padilla, Carlos E Galván-Tejada, Francisco Eneldo López-Monteagudo, Omero Alonso-González, Arturo Moreno-Báez, Antonio Martínez-Torteya, Jorge I Galván-Tejada, Jose G Arceo-Oлагue, Huizilopoztl Luna-García, and Hamurabi Gamboa-Rosales. Speed bump detection using accelerometric features: A genetic algorithm approach. *Sensors*, 18(2):443, 2018.

[10] Amir Salman and Adnan Noor Mian. Deep learning based speed bumps detection and characterization using smartphone sensors. *Pervasive and Mobile Computing*, 92:101805, 2023.

[11] Yunfei Yin, Wanli Fu, Xianyong Ma, Junpeng Yu, Xinkai Li, and Zejiao Dong. Road surface pits and speed bumps recognition based on acceleration sensor. *IEEE Sensors Journal*, 24(7):10669–10679, 2024.

[12] Abiel Aguilar-González and Alejandro Medina Santiago. Road event detection and classification algorithm using vibration and acceleration data. *Algorithms*, 18(3):127, 2025.

[13] Sompote Youwai, Achitaphon Chaiyaphat, and Pawarotorn Chaipetch. Yolo9tr: a lightweight model for pavement damage detection utilizing a generalized efficient layer aggregation network and attention mechanism. *Journal of Real-Time Image Processing*, 21(5):163, 2024.

[14] Sung-Sik Park, Van-Than Tran, and Dong-Eun Lee. Application of various yolo models for computer vision-based real-time pothole detection. *Applied Sciences*, 11(23):11229, 2021.

[15] Muhammad Haroon Asad, Saran Khaliq, Muhammad Haroon Yousaf, Muhammad Obaid Ullah, and Afaq Ahmad. Pothole detection using deep learning: A real-time and ai-on-the-edge perspective. *Advances in Civil Engineering*, 2022(1):9221211, 2022.

[16] Malhar Khan, Muhammad Amir Raza, Ghulam Abbas, Salwa Othmen, Amr Yousef, and Touqeer Ahmed Jumani. Pothole detection for autonomous vehicles using deep learning: a robust and efficient solution. *Frontiers in Built Environment*, 9:1323792, 2024.

[17] Boris Bučko, Eva Lieskovská, Katarína Zábovská, and Michal Zábovský. Computer vision based pothole detection under challenging conditions. *Sensors*, 22(22):8878, 2022.

[18] N Bhavana, Mallikarjun M Kodabagi, B Muthu Kumar, P Ajay, N Muthukumaran, and A Ahilan. Pot-yolo: Real-time road potholes detection using edge segmentation-based yolo v8 network. *IEEE Sensors Journal*, 24(15):24802–24809, 2024.

[19] Jinwang Wang, Chang Xu, Wen Yang, and Lei Yu. A normalized gaussian wasserstein distance for tiny object detection. *arXiv preprint arXiv:2110.13389*, 2021.

[20] Qi Wang, Lu Liu, Wenxin Yu, Shiyu Chen, Jun Gong, and Peng Chen. Bckd: block-correlation knowledge distillation. In *2023 IEEE International Conference on Image Processing (ICIP)*, pages 3225–3229. IEEE, 2023.

[21] Alexander Buslaev, Vladimir I Iglovikov, Eugene Khvedchenya, Alex Parinov, Mikhail Druzhinin, and Alexandr A Kalinin. Albumentations: fast and flexible image augmentations. *Information*, 11(2):125, 2020.

[22] Rahima Khanam and Muhammad Hussain. Yolov11: An overview of the key architectural enhancements. *arXiv preprint arXiv:2410.17725*, 2024.

[23] Kai Han, Yunhe Wang, Qi Tian, Jianyuan Guo, Chunjing Xu, and Chang Xu. Ghostnet: More features from cheap operations. In *Proceedings of the IEEE/CVF conference on computer vision and pattern recognition*, pages 1580–1589, 2020.

[24] Ningning Ma, Xiangyu Zhang, Hai-Tao Zheng, and Jian Sun. Shufflenet v2: Practical guidelines for efficient cnn architecture design. In *Proceedings of the European conference on computer vision (ECCV)*, pages 116–131, 2018.

[25] Danfeng Qin, Chas Leichner, Manolis Delakis, Marco Fornoni, Shixin Luo, Fan Yang, Weijun Wang, Colby Banbury, Chengxi Ye, Berkin Akin, et al. Mobilenetv4: Universal models for the mobile ecosystem. In *European Conference on Computer Vision*, pages 78–96. Springer, 2024.

[26] Hulin Li, Jun Li, Hanbing Wei, Zheng Liu, Zhenfei Zhan, and Qiliang Ren. Slim-neck by gsconv: A lightweight design for real-time detector architectures. *Journal of Real-Time Image Processing*, 21(3):62, 2024.

- [27] S Nienaber, MJ Booysen, and RS Kroon. Detecting potholes using simple image processing techniques and real-world footage. Southern African Transport Conference, 2015.
- [28] VSKP Varma, S Adarsh, KI Ramachandran, and Binoy B Nair. Real time detection of speed hump/bump and distance estimation with deep learning using gpu and zed stereo camera. *Procedia computer science*, 143:988–997, 2018.
- [29] José-Eleazar Peralta-López, Joel-Artemio Morales-Viscaya, David Lázaro-Mata, Marcos-Jesús Villaseñor-Aguilar, Juan Prado-Olivarez, Francisco-Javier Pérez-Pinal, José-Alfredo Padilla-Medina, Juan-José Martínez-Nolasco, and Alejandro-Israel Barranco-Gutiérrez. Speed bump and pothole detection using deep neural network with images captured through zed camera. *Applied Sciences*, 13(14):8349, 2023.
- [30] Changyong Shu, Yifan Liu, Jianfei Gao, Zheng Yan, and Chunhua Shen. Channel-wise knowledge distillation for dense prediction. In *Proceedings of the IEEE/CVF international conference on computer vision*, pages 5311–5320, 2021.
- [31] Glenn Jocher, Alex Stoken, Jirka Borovec, Liu Changyu, Adam Hogan, Laurentiu Diaconu, Jake Poznanski, Lijun Yu, Prashant Rai, Russ Ferriday, et al. ultralytics/yolov5: v3. 0. *Zenodo*, 2020.
- [32] Chuyi Li, Lulu Li, Hongliang Jiang, Kaiheng Weng, Yifei Geng, Liang Li, Zaidan Ke, Qingyuan Li, Meng Cheng, Weiqiang Nie, et al. Yolov6: A single-stage object detection framework for industrial applications. *arXiv preprint arXiv:2209.02976*, 2022.
- [33] Mupparaju Sohan, Thotakura Sai Ram, and Ch Venkata Rami Reddy. A review on yolov8 and its advancements. In *International Conference on Data Intelligence and Cognitive Informatics*, pages 529–545. Springer, 2024.
- [34] Chien-Yao Wang, I-Hau Yeh, and Hong-Yuan Mark Liao. Yolov9: Learning what you want to learn using programmable gradient information. In *European conference on computer vision*, pages 1–21. Springer, 2024.
- [35] Ao Wang, Hui Chen, Lihao Liu, Kai Chen, Zijia Lin, Jungong Han, et al. Yolov10: Real-time end-to-end object detection. *Advances in Neural Information Processing Systems*, 37:107984–108011, 2024.
- [36] Martin Chileshe, Mayumbo Nyirenda, and John Kaoma. Early detection of sexually transmitted infections using yolo 12: A deep learning approach. *Open Journal of Applied Sciences*, 15(4):1126–1144, 2025.
- [37] Melody Zhou. tensorrt pro-yolov8. https://github.com/Melody-Zhou/tensorRT_Pro-YOL0v8. Accessed July 31, 2025.